05179-4-P

THE UNIVERSITY OF MICHIGAN

COLLEGE OF ENGINEERING
DEPARTMENT OF AERONAUTICAL AND ASTRONAUTICAL ENGINEERING
AIRCRAFT PROPULSION LABORATORY

Quarterly Progress Report No. 4
(1 March 1963 to 31 May 1963)

The Feasibility of a Rotating Detonation Wave Rocket Motor

410035

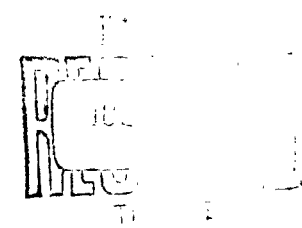

Under contract with:

Air Force Flight Test Center
6593d Test Group (Development)
Contract No. AF 04(611)-8503
Edwards Air Force Base, California

Administered through:

June 1963

OFFICE OF RESEARCH ADMINISTRATION · ANN ARBOR

THE UNIVERSITY OF MICHIGAN

COLLEGE OF ENGINEERING
Department of Aeronautical and Astronautical Engineering
Aircraft Propulsion Laboratory

Quarterly Progress Report No 4
(1 March 1963 to 31 May 1963)

THE FEASIBILITY OF A ROTATING DETONATION WAVE ROCKET MOTOR

ORA Project 05179

under contract with:

AIR FORCE FLIGHT TEST CENTER
6593d TEST GROUP (DEVELOPMENT)
CONTRACT NO AF 04(611)-8503
EDWARDS AIR FORCE BASE, CALIFORNIA

administered through:

OFFICE OF RESEARCH ADMINISTRATION ANN ARBOR

June 1963

TABLE OF CONTENTS

LIST OF FIGURES

LIST OF FIGURES (continued)

NOMENCLATURE - PART I

A	variable used in variation of parameter solution to the injection dynamical equation
A_1	constant of integration
A_c (ft^2)	chamber cross section area, $\ell_c x_n$
A_i (ft^2)	area of an injector orifice
a (ft/sec)	local speed of sound
B	area ratio parameter, $\left(\frac{2}{\gamma + 1}\right)^{\frac{\gamma + 1}{2(\gamma - 1)}} \frac{\ell_t L}{A_c}$
$C_p \left(\frac{\text{ft-lb}}{\text{slug} - {}^\circ\text{R}}\right)$	specific heat at constant pressure
C_{P_ℓ}	injector orifice pressure loss coefficient
F (lb)	axial rocket engine thrust
G	redefined in this report as the mass flow fraction of gaseous propellant
g_c (lbm/slug)	unit conversion constant (32.174)
I_{sp} (sec)	theoretical specific impulse
J	integral defined in the derivation of the jump conditions for the cryogenic case
K	proportionality constant in the parabolic approximation to $\overline{P}(\eta)$
L (ft)	distance between detonation waves, $2\pi R/N$
ℓ_c (ft)	radial width of the chamber
ℓ_i (ft)	characteristic injector orifice length
ℓ_t (ft)	width of the nozzle throat
$\mathcal{M}$ ($mole^{-1}$)	molecular weight
M	Mach number, v/a
$\dot{m}\left(\frac{\text{slugs}}{\text{sec}}\right)$	mass flow rate
$\dot{m}_G\left(\frac{\text{slugs}}{\text{sec}}\right)$	mass flow rate of gaseous propellant

$\dot{m}_\ell \left(\frac{\text{slugs}}{\text{sec}}\right)$	mass flow rate of liquid propellant
$\dot{m}_p \left(\frac{\text{slugs}}{\text{sec}}\right)$	total propellant mass flow rate
N	number of waves in the engine
N_i	number of injector orifices
P, P_c (lbs/ft^2)	instantaneous detonation chamber pressure
P_a (lbs/ft^2)	atmospheric pressure
P_{avg} (lbs/ft^2)	mean detonation chamber pressure
P_D (lbs/ft^2)	injector plenum pressure
P_e (lbs/ft^2)	nozzle exit pressure
ΔP (lbs/ft^2)	total pressure drop across an injector orifice
R (ft)	radius of curvature of the chamber centerline
T ($^\circ$R)	absolute temperature
t (sec)	time
u, v, x	dummy variables of integration
V (ft/sec)	magnitude of the velocity
V_w (ft/sec)	absolute detonation wave velocity
v, u (ft/sec)	circumferential and axial velocity components
V_i (ft/sec)	injection velocity of the liquid propellant
$V_{i\,avg}$	mean value of V_i
X_G	mole fraction of gaseous propellant
x, y (ft)	axial and circumferential coordinates
$y_o(t)$, $y_1(t)$ (ft)	circumferential coordinates of the boundaries of a control volume moving with the fluid
α, β, ω	constants appearing in the differential equation for ϕ
γ	ratio of specific heats

NOMENCLATURE - PART I (continued)

$\zeta(t)$ (ft)	circumferential coordinates of the detonation wave
η	dimensionless circumferential coordinate, y/L
ξ	dimensionless axial coordinate, x/x_n
$\rho \left(\frac{\text{slugs}}{\text{ft}^3}\right)$	mass density
ϕ	nondimensional perturbation in the liquid injection velocity, V_i

Subscripts

0	refers to condition at y = 0
1	refers to condition at y = L
a	refers to absolute velocity
A	refers to the unburned propellant
B	refers to the burned propellant
G	refers to the gaseous propellant
ℓ	refers to the liquid propellant
n	refers to condition at beginning of nozzle
p	refers to the initial propellant condition
t	refers to condition at nozzle throat
w	refers to the detonation wave
$\bar{f}$	denotes f/f_o

Note: Absence of subscript refers to the local condition in the chamber for the wave fixed system of coordinates.

FOREWORD

This report is the Fourth Quarterly Progress Report, 1 March 1963 to 31 May 1963, on Contract No. AF 04(611)-8503, a contract between Edwards Air Force Base and The University of Michigan. The aim of this contract is to investigate the feasibility of a rotating detonation wave rocket motor.

Personnel associated with the various phases of the program as they are divided in the report are as follows:

I. G. Olsson

II. A - G. L. Cosens, K. Ragland, J. Brown, S. Schmidt
B - E. Kurath
C - G. L. Cosens, F. Cheslak, S. Schmidt

This project is directed by Professors J. A. Nicholls and R. E. Cullen of The University of Michigan. The Air Force Project Engineer is Richard Weiss (DGRR), 6593d Test Group (Development), Edwards Air Force Base, California.

SUMMARY

This report presents the work accomplished on the rotating detonation wave engine feasibility program during the period 1 March 1963 to 31 May 1963.

The work described in this report represents essentially the conclusion of the supporting experimental and theoretical studies intended to consume approximately the first half of the program. The last half of the program will emphasize the testing of a nominal 1000 lb-thrust, rocket motor utilizing the detonative mode of combustion and employing hydrogen and oxygen as the propellants.

The theoretical studies of an analytical model for the internal gas dynamics associated with a rotating detonation wave engine have been essentially completed.

The numerical computations to solve the differential equations for the analytical model have been carried out for the no mixing case for initial propellant temperatures of $537^{\circ}R$ and $270^{\circ}R$ plots of the various dimensionless gas dynamic parameters versus the dimensionless circumferential coordinate, η, are shown. A modification of the analytical model to handle the case of one propellant injected as a liquid is presented. Work on carrying out the necessary numerical computations is in progress. An expression for the specific impulse of the idealized rotating detonation wave engine has been obtained. Comparison with the ideal conventional rocket engine shows that the vacuum specific impulse is essentially the same for both cases. A list of sizing rules derived from the analytical model are presented.

The experimental supporting studies have been essentially completed. Work is continuing on the gaseous 100-lb thrust motor

(1) All attempts to start the 100-lb thrust motor have proven unsuccessful, therefore, a linear motor, similar in other respects to the 100-lb thrust motor, and having transparent combustion chamber walls has been fabricated to study the problem systematically.

(2) The experiments concerning detonations in heterogeneous, liquid-gas media have been extended to include the case of the shattering of smaller (220 - 580 μ) H_2O droplets behind detonation waves. It appears that these droplets break up in the same manner and time interval (~ 10 μ sec) as the 1000 μ droplets studied earlier. The appearance of a detached normal shock wave upstream of the row of shattered droplets is noted for this case.

(3) The experiments concerning the effect of curvature and pressure relief has yielded two conclusions. First, in general it appears that in curved channels (of the same approximate dimensions as that employed in the experiments) detonation waves will propagate at velocities (measured at the channel centerline) equal to that observed in straight tubes. Secondly, with no confinement (pressure relief) on the inner wall, measured detonation velocities in the curved channel appear to suffer a degradation of no more than 7.5% compared to the measured velocities of completely confined waves.

I. ANALYTICAL MODEL OF THE ROTATING DETONATION WAVE ENGINE

A. INTRODUCTION

In References 1 and 2 a simplified model of the rotating detonation wave engine was developed. A numerical solution to the case of complete instantaneous mixing between the burned and unburned propellants was given in Reference 2. In the present report numerical solutions to the case of no mixing between the burned and unburned propellants are also presented.

In addition, the analytical model has been modified to include the case of one propellant being injected in the liquid state. The injection dynamics for a liquid propellant are analyzed and sizing rules for injector design are derived.

The analytical model also has been applied to the calculation of the specific impulse of rotating detonation wave engines. Comparison with the specific impulse of conventional engines indicates that an ideal rotating wave engine has the same vacuum specific impulse as an equivalent steady conventional rocket engine, but that mixing between the burned and unburned propellants or inefficiencies in exit nozzle performance would cause a degradation in specific impulse.

Also, the sizing rules for engine design derived from the analytical model are summarized for convenient reference.

B. RESULTS OF A NUMERICAL SOLUTION TO THE NO MIXING CASE

A digital computer program to integrate numerically the differential equations for the no mixing case (see References 1 and 2) has been developed. The results for stoichiometric gaseous hydrogen-oxygen injected at $537^{\circ}R$ and $270^{\circ}R$ are presented in Figures 1 and 2, respectively.

Compared to the complete mixing case the temperature of the gases entering the detonation wave for the no mixing case is lower and represents the ideal case of a detonation propagating in an unburned media. Note that the

velocities v_A and v_B are measured relative to the wave fixed coordinates.

C. APPLICATION OF THE ANALYTICAL MODEL TO THE CRYOGENIC CASE

An important problem to analyze is the situation where one propellant is injected into the detonation chamber in the liquid state (for example, liquid oxygen and gaseous hydrogen as propellants). For the simplified analysis given here, only the jump conditions across the detonation wave and the definition of certain parameters need to be modified in the original model of the no mixing case.

Assumptions

1. The no mixing model is to be used as the basis of the analysis.
2. In control volume A one propellant is in the liquid state, the other is in the gaseous state. The volume of the liquid is neglected compared to the volume of the gas.
3. There is no interaction between the liquid drops and the gaseous propellant, i. e., the circumferential coordinate of the drops remains stationary with respect to the engine.
4. The liquid propellant evaporates and reacts instantaneously at the plane of the detonation wave.

Control volume A will effectively contain only gaseous propellant since the liquid occupies negligible volume and is assumed not to interact with the gaseous propellant. Hence the differential equations derived for the all-gaseous case will remain valid, except that the parameters γ_A, $\overline{C}_{P_A}$, G, and $\overline{T}_P$ will need to be redefined.

At the detonation wave there is a source of vaporizing propellant. Consequently, the hydrodynamic jump conditions across the detonation wave need modification.

Detonation Wave Jump Conditions Including a Source of Vaporizing Propellant

The derivation of the jump conditions given here follows the method presented in Reference 3.

Consider a control volume moving with the fluid. Within the control volume there is a detonation wave immediately preceded by a source of vaporizing propellant. The following is a schematic view of this system with respect to the wall fixed coordinates (see page 13 of Reference 1):

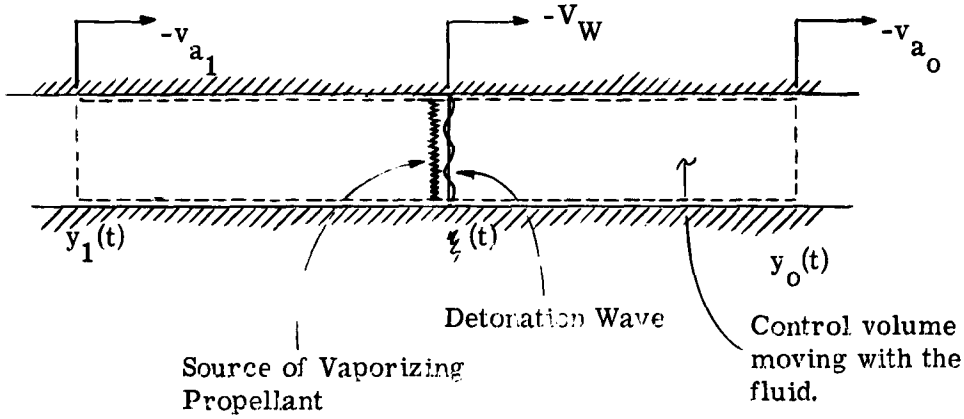

The conservation equations of mass and momentum for the control volume moving with the fluid are

$$\frac{d}{dt}\int_{y_1(t)}^{y_0(t)} \rho \, dy = \frac{\dot{m}_\ell}{NA_c}$$

$$\frac{d}{dt}\int_{y_1(t)}^{y_0(t)} \rho \, (-v_a) \, dy = P_1 - P_0$$

Note that the integrals are of the form

$$J = \int_{y_1(t)}^{y_0(t)} \psi(y,t)\, dy$$

therefore,

$$\frac{dJ}{dt} = \frac{d}{dt} \int_{y_1(t)}^{\zeta(t)} \psi(y,t)\, dy + \frac{d}{dt} \int_{\zeta(t)}^{y_0(t)} \psi(y,t)\, dy$$

$$= \int_{y_1(t)}^{y_0(t)} \frac{\partial \psi}{\partial t}\, dy + \psi(\zeta^{(-)}, t)\, \dot{\zeta} - \psi(y_1, t)\, \dot{y}_1$$

$$+ \psi(y_0, t)\, \dot{y}_0 - \psi(\zeta^{(+)}, t)\, \dot{\zeta}$$

$$\lim_{(y_0 - y_1) \to 0} \frac{dJ}{dt} = \psi_0 (V_w - v_{a_0}) - \psi_1 (V_w - v_{a_1})$$

Utilizing the velocity transformation from the wall fixed coordinates to a coordinate system moving with the detonation wave,

$$v = V_w - v_a$$

one obtains

$$\lim_{(y_0 - y_1) \to 0} \frac{dJ}{dt} = \psi_0 v_0 - \psi_1 v_1$$

The continuity equation becomes, with $\psi = \rho$,

$$\rho_1 v_1 + \frac{\dot{m}_\ell}{NA_c} = \rho_0 v_0$$

For the momentum equation, $\psi = -\rho v_a$. Therefore,

$$-\rho_0 v_0 (V_w - v_0) + \rho_1 v_1 (V_w - v_1) = P_1 - P_0$$

Combination with the continuity equation yields

$$P_1 + \rho_1 v_1^2 + \frac{\dot{m}_\ell}{NA_c} V_w = P_0 + \rho_0 v_0^2$$

Non-Dimensional Form of the Jump Conditions

In non-dimensional form the continuity jump condition becomes

$$\overline{\rho}_{A_1} \overline{v}_{A_1} + \overline{\dot{m}}_\ell = 1$$

where $\overline{\dot{m}}_\ell$ is defined as

$$\overline{\dot{m}}_\ell = \frac{\dot{m}_\ell}{\rho_{B_0} v_{B_0} NA_c}$$

Previously, the mass flow parameter G was defined by

$$G = \frac{\dot{m}_P}{\rho_{B_0} v_{B_0} NA_c}$$

where $\dot{m}_P$ is the total propellant mass flow rate. The above relation, with G = 1, can be viewed as a definition of A_c, since A_c in the analysis represents an effective detonation wave area rather than a chamber cross-sectional area. Also,

$$\dot{m}_P = \dot{m}_G + \dot{m}_\ell$$

Redefine G by the relation

$$G = \frac{\dot{m}_G}{\rho_{B_0} v_{B_0} NA_c}$$

Hence one obtains the relationships

$$\bar{\rho}_{A_1} \bar{v}_{A_1} = G$$

$$\bar{\dot{m}}_\ell = 1 - G$$

The non-dimensional form of the momentum equation is

$$\bar{P}_1 + \gamma_B \bar{\rho}_1 \bar{v}_{A_1}^2 + \gamma_B \bar{\dot{m}}_\ell \bar{V}_w = \gamma_B + 1$$

From the definition of G this becomes

$$\bar{P}_1 + \gamma_B G \bar{v}_{A_1} + \gamma_B (1 - G) \bar{V}_w = \gamma_B + 1$$

In terms of mole fractions G is expressed as

$$G = \frac{\mathcal{M}_G X_G}{\mathcal{M}_G X_G + \mathcal{M}_\ell (1 - X_G)}$$

where X_G is the mole fraction of gaseous propellant.

To solve for $\bar{P}_1$, $\bar{v}_{A_1}$, and M_{A_1}, the integrated energy equation for control volume A (see Reference 1, page 27) is required:

$$\frac{\gamma_B - 1}{\gamma_A - 1} \bar{a}_{A_1}^2 + \frac{\gamma_B - 1}{2} \bar{v}_{A_1}^2 = \bar{C}_{P_A} \bar{T}_P + \frac{\gamma_B - 1}{2} \bar{V}_w^2$$

Note that in this case γ_A and C_{P_A} refer to the specific heat ratio and specific heat for the gaseous propellant in control volume A, G refers to the mass fraction of gaseous propellant, and T_P refers to the injection temperature of the gaseous propellant.

Combination of this energy equation with the continuity and momentum jump relations yields

$$\bar{v}_{A_1} = r + \sqrt{r^2 - \frac{2}{\gamma_A + 1}\left\{\frac{\gamma_A - 1}{\gamma_B - 1} C_{P_A} \bar{T}_P + \frac{\gamma_A - 1}{2} \bar{V}_w^2\right\}}$$

where r is defined by

$$r = \frac{\gamma_A}{\gamma_B G}\left[\frac{1 - \gamma_B\left[(1 - G)\,\bar{V}_w - 1\right]}{\gamma_A + 1}\right]$$

$$\bar{P}_1 = 1 - \gamma_B\left[G\,\bar{v}_{A_1} + (1 - G)\,\bar{V}_w - 1\right]$$

$$M_{A_1} = \frac{\overline{\gamma_B G\,\bar{v}_{A_1}}}{\gamma_A \bar{P}_1}$$

In the numerical solution to this problem the thermochemical calculations of Reference 4 will be used. Note that the heat of vaporization of the liquid propellant modifies the initial temperature used in applying the thermochemical results.

Work on a digital computer program to solve these equations for the cryogenic case is in progress.

D. INJECTION DYNAMICS FOR A LIQUID PROPELLANT

An important aspect of engine design is the dynamics of the injection of liquid propellants. It is necessary to insure the injector design will provide the desired mass flow rate of liquid propellant and also distribute the liquid across the axial dimension of the detonation chamber. The injector is assumed to consist of a large number of holes of the form

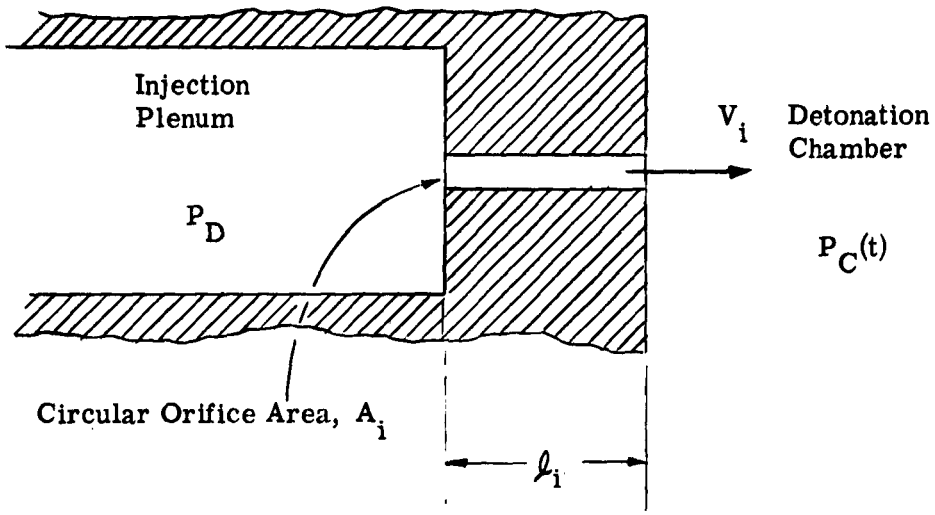

Following an approach used by Morrison, * for steady flow through this system the pressure loss coefficient C_{P_ℓ} is given by

$$C_{P_\ell} = \frac{\Delta P}{\frac{1}{2}\rho_\ell V^2}$$

where ΔP is the loss in total pressure from the point where P_D is imposed to the point where P_C exists; V is a characteristic velocity. Choose the injection velocity V_i to be the characteristic velocity. Then C_{P_ℓ} is given by

$$C_{P_\ell} = \frac{P_D - P_C - \frac{1}{2}\rho_\ell V_i^2}{\frac{1}{2}\rho_\ell V_i^2}$$

for steady flow.

The momentum contained in the orifice at an instant in time is $\rho_\ell A_i \ell_i V_i$. Hence the pressure head due to the inertia of the fluid is $\rho_\ell \ell_i \, d V_i/dt$, and the pressure loss coefficient for the unsteady flow case can be written as

*Unpublished analysis made at this laboratory by R. B. Morrison.

$$C_{P_\ell} = \frac{P_D - P_C(t) - \frac{1}{2}\rho_\ell V_i^2 - \rho_\ell \ell_i \, d V_i/dt}{\frac{1}{2}\rho_\ell V_i^2}$$

As an approximation assume C_{P_ℓ} is constant with time.

Note that the only justification of the assumptions employed here is that they provide a basis for obtaining a simple solution to the problem.

For the rotating detonation wave engine, however, P_C fluctuates very rapidly with time, while P_D may be assumed constant. (Here Morrison assumed $(P_D - P_C)$ constant.) The differential equation for $V_i(t)$ is then

$$\frac{dV_i}{dt} + \frac{1 + C_{P_\ell}}{2\ell_i} V_i^2 = \frac{P_D - P_C(t)}{\rho_\ell \ell_i}$$

To put this equation in non-dimensional form introduce

$$\bar{P}_D = P_D/P_0, \qquad \bar{P} = P_C/P_0, \qquad \eta = V_w t/L$$

$$\bar{V}_i = V_i/v_{B_0}, \qquad \bar{\rho}_\ell = \rho_\ell/\rho_{B_0}, \qquad \bar{\ell}_i = \ell_i/L$$

resulting in

$$\frac{d\bar{V}_i}{d\eta} + \frac{1 + C_{P_\ell}}{2\bar{V}_w \bar{\ell}_i} \bar{V}_i^2 = \frac{\bar{P}_D - \bar{P}(\eta)}{\gamma_B \bar{\rho}_\ell \bar{\ell}_i \bar{V}_w}$$

It has been found that $\bar{P}(\eta)$ can be closely approximated by a parabola of the form

$$\bar{P}(\eta) = 1 - K\eta^{1/2}$$

where K is a constant (e. g., $K \approx 1 - \bar{P}_1$).

The boundary condition is

$$\bar{V}_i(0) = \bar{V}_i(1)$$

Since the equation is non linear an exact solution would require numerical integration, for example by the Runge-Kutta procedure. To obtain some insight into the effects of injection dynamics, a perturbation solution to the differential equation is obtained.

Define $\phi(\eta)$ as the fluctuation in $\bar{V}_i$ from the mean value $\bar{V}_{i\,avg}$.

$$\phi = \bar{V}_i - \bar{V}_{i\,avg}$$

Assume $\phi/\bar{V}_{i\,avg} << 1$. This is equivalent to assuming $\bar{P}_D >> 1$.

The differential equation for ϕ is

$$\frac{d\phi}{d\eta} + \omega\phi = \alpha + \beta\eta^{1/2}$$

where $\omega = \dfrac{(1 + C_{P_\ell})\,\bar{V}_{i\,avg}}{\bar{\ell}_i\,\bar{V}_w}$

$$\alpha = -\frac{(1 + C_{P_\ell})\,\bar{V}_{i\,avg}^{\,2}}{2\,\bar{\ell}_i\,\bar{V}_w} + \frac{\bar{P}_D - 1}{\gamma_B\,\bar{\rho}_\ell\,\bar{\ell}_i\,\bar{V}_w}$$

$$\beta = \frac{K}{\gamma_B\,\bar{\rho}_\ell\,\bar{\ell}_i\,\bar{V}_w}$$

This differential equation can be solved by the method of variation of parameters. The solution to the homogeneous equation

$$\frac{d\phi}{d\eta} + \omega\phi = 0$$

is

$$\phi = Ae^{-\omega\eta}$$

Let $A = A(\eta)$ and substitute into the non-homogeneous equation:

$$e^{-\omega\eta}\frac{dA}{d\eta} - \omega A e^{-\omega\eta} + \omega A e^{-\omega\eta} = \alpha + \beta\eta^{1/2}$$

$$\frac{dA}{d\eta} = \alpha e^{\omega\eta} + \beta\eta^{1/2}\, e^{\omega\eta}$$

$$A = \frac{\alpha}{\omega} e^{\omega\eta} + \beta \int_0^{\eta} x^{1/2}\, e^{\omega x}\, dx + A_1$$

where A_1 is a constant of integration. Hence ϕ is given by

$$\phi(\eta) = \frac{\alpha}{\omega} + \beta\, e^{-\omega\eta} \int_0^{\eta} x^{1/2}\, e^{\omega x}\, dx + A_1\, e^{-\omega\eta}$$

A_1 is evaluated from the boundary condition $\phi(0) = \phi(1)$:

$$\frac{\alpha}{\omega} + A_1 = \frac{\alpha}{\omega} + \beta\, e^{-\omega} \int_0^{1} x^{1/2}\, e^{\omega x}\, dx + A_1\, e^{-\omega}$$

$$A_1 = \left(\frac{\beta}{e^{\omega} - 1}\right) \int_0^{1} x^{1/2}\, e^{\omega x}\, dx$$

Therefore, the solution for ϕ is

$$\phi(\eta) = \frac{\alpha}{\omega} + \beta\, e^{-\omega\eta} \int_0^{\eta} x^{1/2}\, e^{\omega x}\, dx + \frac{\beta\, e^{-\omega\eta}}{e^{\omega} - 1} \int_0^{1} x^{1/2}\, e^{\omega x}\, dx$$

From the definition of $\overline{V}_{i\ avg}$,

$$\int_0^1 \phi \, d\eta = 0$$

or,

$$\frac{\alpha}{\omega} + \beta \int_0^1 e^{-\omega\eta} \int_0^\eta x^{1/2} \, e^{\omega x} \, dx \; d\eta + \frac{\beta}{\omega e^{\omega}} \int_0^1 x^{1/2} \, e^{\omega x} \, dx = 0$$

The second term can be evaluated by applying the relation

$$\int_0^1 u \, dv = u \, v \Big|_0^1 - \int_0^1 v \, du$$

resulting in

$$\alpha + \frac{2}{3} \beta = 0$$

or,

$$- \frac{(1 + C_{P_\ell}) \, \overline{V}_{i \, avg}^{\,2}}{2 \, \overline{\ell}_i \, \overline{V}_w} + \frac{\overline{P}_P - 1 + \frac{2}{3} K}{\gamma_B \, \overline{\rho}_\ell \, \overline{\ell}_i \, \overline{V}_w} = 0$$

$$\overline{V}_{i \, avg} = \sqrt{\frac{2 \left[\overline{P}_D - 1 + \frac{2}{3} K \right]}{\gamma_B \, \overline{\rho}_\ell \, (1 + C_{P_\ell})}}$$

Note that the quantity 1 - 2K/3 represents a mean chamber pressure, since

$$\overline{P}_{avg} = \int_0^1 \overline{P}\, d\eta = \int_0^1 (1 - K\eta^{1/2})\, d\eta = 1 - \frac{2}{3} K$$

Hence K can best be found from $K = 1.5\,(1 - \overline{P}_{avg})$ where $\overline{P}_{avg}$ is the area under the $\overline{P}(\eta)$ versus η curve obtained from the engine analytical model.

For steady flow through the injector

$$C_{P_\ell} = \frac{P_D - P_{C\,avg} - \frac{1}{2}\rho_\ell V_{i\,avg}^2}{\frac{1}{2}\rho_\ell V_{i\,avg}^2}$$

or,

$$\overline{V}_{i\,avg} = \sqrt{\frac{2\left[\overline{P}_D - \overline{P}_{avg}\right]}{\gamma_B \bar{\rho}_\ell (1 + C_{P_\ell})}}$$

In the linearized case the mean injection velocity does not differ from the steady state value. To judge the unsteady effect on $\overline{V}_{i\,avg}$ a solution to the non-linear differential equation should be obtained.

Sizing Laws Derived from the Liquid Injection Analysis

Using the derived relation for $\overline{V}_{i\,avg}$ one can express the following sizing relations in quantitative form.

1. The total mass flow rate of liquid through the injector should equal $\dot{m}_\ell$. Therefore,

$$m_\ell = \rho_\ell N_i A_i V_{i\,avg}$$

where N_i is the number of injector orifices and A_i is the area of each orifice. In non-dimensional form this becomes

$$\bar{\dot{m}}_\ell = \frac{\bar{\rho}_\ell \, N_i \, A_i \, \bar{V}_{i\,avg}}{NA_c}$$

or,

$$\bar{\dot{m}}_\ell = \frac{N_i \, A_i}{NA_c} \sqrt{\frac{2\bar{\rho}_\ell \, [\bar{P}_D - \bar{P}_{avg}]}{\gamma_B \, (1 + C_{P_\ell})}}$$

2. The injected liquid should move a distance x_n in the same time the detonation wave travels a distance L. Hence

$$\frac{x_n}{V_{i\,avg}} = \frac{L}{V_w}$$

or,

$$\bar{x}_n = \frac{V_{i\,avg}}{V_w} \qquad (\bar{x}_n = x_n/L)$$

$$\bar{x}_n = \frac{1}{\bar{V}_w} \sqrt{\frac{2 \, [\bar{P}_D - \bar{P}_{avg}]}{\gamma_B \, \bar{\rho}_\ell \, (1 + C_{P_\ell})}}$$

E. THEORETICAL SPECIFIC IMPULSE OF ROTATING DETONATION WAVE ENGINES

To derive the relation for the specific impulse of the rotating detonation wave engine the well known steady flow analysis for conventional rocket engines is applied to calculate the thrust of an infinitesimal segment of the engine. The result is integrated over the circumference of the engine and division by the propellant mass flow rate yields an expression for the overall specific impulse. It is assumed that the flow in the nozzle is expanded ideally to a given exit pressure P_e.

Specific Impulse of a Steady Flow Rocket Engine

The specific impulse, I_{sp}, of a rocket engine is defined as the thrust per unit mass flow rate of propellant. It is conventional to use pounds-mass as the unit of mass, then I_{sp} is given in units of seconds. To make the equation dimensionally correct the constant g_c (32.174 lbm/slug) is introduced.

Consider a rocket engine mounted on a test stand:

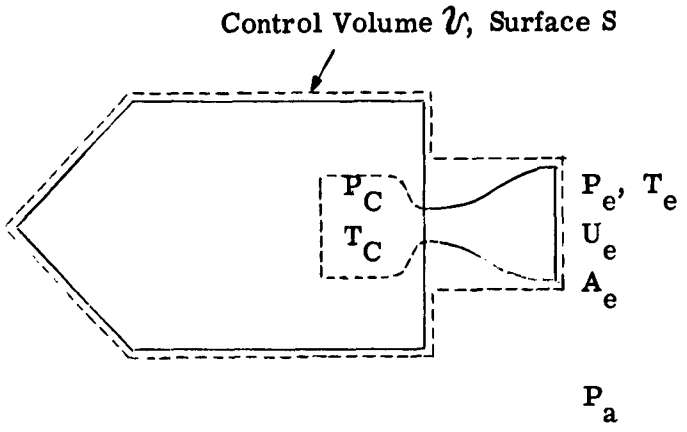

From the momentum theorem for steady flow the rocket thrust is given by

$$\underset{\sim}{F} = \iint_S [\rho \underset{\sim}{V} (\underset{\sim}{V} \cdot \hat{n}) + P\hat{n}] \, dS$$

where $\hat{n}$ is the local outward unit normal vector to the element of surface area, dS. For the control volume $\mathcal{V}$ one obtains for the magnitude of the thrust

$$F = \rho_e u_e^2 A_e + (P_e - P_a) A_e$$

and since the propellant mass flow rate $\dot{m}_P$ equals $\rho_e u_e A_e$, the specific impulse is

$$I_{sp} = F/\dot{m}_P g_c = \frac{u_e}{g_c} + \frac{(P_e - P_a) A_e}{\dot{m}_P g_c}$$

The nozzle exit velocity u_e is found from the energy equation

$$C_P T_e + \frac{1}{2} u_e^2 = C_P T_c$$

and the relation for isentropic nozzle flow,

$$\frac{T_e}{T_c} = \left(\frac{P_e}{P_c}\right)^{\frac{\gamma - 1}{\gamma}}$$

Hence the result for u_e is

$$u_e = \sqrt{2 C_P T_c \left[1 - \left(\frac{P_e}{P_c}\right)^{\frac{\gamma - 1}{\gamma}}\right]}$$

Specific Impulse of a Rotating Detonation Wave Engine

To apply the steady flow specific impulse relation to a rotating detonation wave engine, consider the flow field in the wave fixed coordinate system. The flow is steady, then the nozzle flow can be represented ideally as consisting of a large number of infinitesimal steady engines. Note that the axial velocity component, u, has the same value in both the wall fixed and wave fixed coordinate systems and hence that the thrust calculation can be performed in either reference system. Consider one such incremental steady engine. The energy relation is

$$C_{P_B} T_e + \frac{1}{2} u_e^2 = C_{P_B} T_B$$

Note that now T_B depends upon the detonation chamber circumferential coordinate y. Also, for isentropic flow in the nozzle,

$$\frac{T_e}{T_B} = \left(\frac{P_e}{P}\right)^{\frac{\gamma_B - 1}{\gamma_B}}$$

hence

$$u_e = \sqrt{2\, C_{P_B}\, T_B \left[1 - \left(\frac{P_e}{P} \right)^{\frac{\gamma_B - 1}{\gamma_B}} \right]}$$

The mass flow rate through an infinitesimal nozzle segment with exit area $\ell_e\, dy$ is (see page 23 of Reference 1)

$$\frac{d\dot{m}_t}{N} = \rho_B\, a_B\, \ell_t \left(\frac{2}{\gamma_B + 1} \right)^{\frac{\gamma_B + 1}{2(\gamma_B - 1)}} dy$$

Hence the thrust of this incremental nozzle segment is

$$dF = \sqrt{2\, C_{P_B}\, T_B \left[1 - \left(\frac{P_e}{P} \right)^{\frac{\gamma_B - 1}{\gamma_B}} \right]}\, \rho_B\, a_B\, \ell_t \left(\frac{2}{\gamma_B + 1} \right)^{\frac{\gamma_B + 1}{2(\gamma_B - 1)}} dy + (P_e - P_a)\, \ell_e\, dy$$

Integrating over the length L between detonation waves and multiplying by the number of waves, one obtains for the specific impulse

$$I_{sp} = \frac{N}{\dot{m}_P\, g_c} \int_0^L \left\{ \sqrt{2\, C_{P_B}\, T_B \left[1 - \left(\frac{P_e}{P} \right)^{\frac{\gamma_B - 1}{\gamma_B}} \right]}\, \rho_B\, a_B\, \ell_t \left(\frac{2}{\gamma_B + 1} \right)^{\frac{\gamma_B + 1}{2(\gamma_B - 1)}} + (P_e - P_a)\, \ell_e \right\} dy$$

Using the relations

$$\dot{m}_p = \rho_{B_0}\, v_{B_0}\, A_c\, N$$

$$B = \frac{\ell_t L}{A_c} \left(\frac{2}{\gamma_B + 1} \right)^{\frac{\gamma_B + 1}{2(\gamma_B - 1)}}$$

the non-dimensional form of the relation is

$$I_{sp} = \frac{1}{g_c} \sqrt{2 C_{P_B} T_{B_0}}\, B \int_0^1 \bar{P} \left[1 - \left(\frac{1}{\bar{P}} \frac{P_e}{P_o} \right)^{\frac{\gamma_B - 1}{\gamma_B}} \right]^{\frac{1}{2}} d\eta$$

$$+ \frac{1}{\gamma_B g_c} \sqrt{(\gamma_B - 1) C_{P_B} T_{B_0}} \left(\frac{\ell_e L}{A_c} \right) \left(\frac{P_a}{P_o} \right) \left(\frac{P_e}{P_a} - 1 \right)$$

There are two special cases of interest:

1. Nozzle exit pressure P_e equals the ambient pressure P_a

$$I_{sp} = \frac{1}{g_c} \sqrt{2 C_{P_B} T_{B_0}}\, B \int_0^1 \bar{P} \left[1 - \left(\frac{1}{\bar{P}} \frac{P_a}{P_o} \right)^{\frac{\gamma_B - 1}{\gamma_B}} \right]^{\frac{1}{2}} d\eta$$

2. Ideal expansion to vacuum conditions ($P_e = 0$)

$$I_{sp\ vac} = \frac{1}{g_c} \sqrt{2 C_{P_B} T_{B_0}}\, B \int_0^1 \bar{P}\, d\eta$$

The analogous expression for a steady flow engine is

$$(I_{sp\ vac})_s = \frac{1}{g_c} \sqrt{2 C_{P_S} T_{C_S}}$$

Hence the ratio of vacuum specific impulse for the rotating detonation wave engine to the value for a steady engine is

$$\frac{(I_{sp\ vac})_{RDWE}}{(I_{sp\ vac})_s} = \sqrt{\frac{C_{P_B} T_{B_0}}{C_{P_S} T_{C_S}}}\, B \int_0^1 \bar{P}\, d\eta$$

This ratio has been found to be essentially unity for the case of no mixing between the burned and unburned propellant. However, there exist two possible causes of performance degradation of the rotating detonation wave engine:

1. Mixing between the burned and unburned propellant
2. Non-ideal nozzle performance.

It is anticipated that the extent of these effects will be evaluated experimentally.

F. SUMMARY OF ENGINE SIZING RULES DERIVED FROM THE ANALYTICAL MODEL—CRYOGENIC CASE

The following is a summary of the sizing rules that have been derived from the analytical model as applied to the no mixing, cryogenic case:

1. Sizing rules from similarity considerations (see Reference 2, page 16).

$$A_c = \frac{\dot{m}_P}{\gamma_B N P_0} \sqrt{(\gamma_B - 1) C_{P_B} T_{B_0}}$$

$$\ell_t = \frac{\dot{m}_P B}{2\pi R \gamma_B P_0} \sqrt{(\gamma_B - 1) C_{P_B} T_{B_0}} \left(\frac{\gamma_B + 1}{2}\right)^{\frac{\gamma_B + 1}{2(\gamma_B - 1)}}$$

Note that G as defined in Reference 2 is unity in this case. Also, there are the definitions

$$L = 2\pi R/N$$

$$A_c = x_n \ell_c$$

2. Sizing rules from propellant injection analysis

$$G = \frac{X_G \mathcal{M}_G}{X_G \mathcal{M}_G + (1 - X_G)\mathcal{M}_\ell}$$

$$\overline{\dot{m}}_\ell = 1 - G$$

$$\overline{\dot{m}}_\ell = \frac{N_i A_i}{N A_c} \sqrt{\frac{2\,\overline{\rho}_\ell \left(\overline{P}_D - \int_0^1 \overline{P}\, d\eta \right)}{\gamma_B (1 + C_{P_\ell})}}$$

$$\frac{x_n}{L} = \frac{1}{\overline{V}_w} \sqrt{\frac{2 \left(\overline{P}_D - \int_0^1 \overline{P}\, d\eta \right)}{\gamma_B \overline{\rho}_\ell (1 + C_{P_\ell})}}$$

$$\overline{V}_{i\,avg} = \sqrt{\frac{2 \left(\overline{P}_D - \int_0^1 \overline{P}\, d\eta \right)}{\gamma_B \overline{\rho}_\ell (1 + C_{P_\ell})}}$$

$$\ell_c \sim x_n$$

3. Sizing rules from performance analysis

$$F = \dot{m}_P \sqrt{2\, C_{P_B}\, T_{B_0}} \left\{ B \int_0^1 \overline{P} \left[1 - \left(\frac{1}{\overline{P}} \frac{P_e}{P_o} \right)^{\frac{\gamma_B - 1}{\gamma_B}} \right]^{\frac{1}{2}} d\eta \right.$$

$$\left. + \frac{1}{\gamma_B} \sqrt{\frac{\gamma_B - 1}{2}} \left(\frac{\ell_e L}{A_c} \right) \left(\frac{P_a}{P_o} \right) \left(\frac{P_e}{P_a} \right) - 1 \right\}$$

Note: T_{B_0} can be found from the results of a thermochemistry calculation for the detonation wave (see Reference 4, for example) instead of utilizing Q and $\overline{Q}$ as indicated in Reference 2. This method is also used to determine the molecular weight and specific heat ratio of the burned propellant.

G. RESULTS AND CONCLUSIONS

The numerical calculations to solve the differential equations for the rotating detonation wave engine analytical model as indicated in References 1 and 2 have been carried out and the results are presented in Figures 1 and 2 of Reference 2 and in Figures 1 and 2 of this report.

A modification of the engine analytical model to handle the case of one propellant being injected as a liquid is presented here. Work on carrying out the necessary numerical computations for this analysis is in progress.

An expression for the specific impulse of the idealized rotating detonation wave engine has been obtained, and comparison with an ideal conventional rocket engine shows that the theoretical vacuum specific impulse is essentially the same for both cases. More detailed comparisons of the relative performance of rotating detonation wave and steady flow engines are being considered.

For convenience, the complete list of sizing rules derived from the analytical model have been summarized.

Besides the remaining numerical computations to be completed, future work concerning the analytical model chiefly involves obtaining correlations with experimental results.

II. EXPERIMENTAL STUDIES

A. THE GASEOUS 100-LB THRUST MOTOR

All attempts to start the 100-lb thrust motor have proven unsuccessful. Numerous starting schemes, including the starting system first used during the 1961 test series, have been tried. These 1961 experiments have been duplicated as nearly as possible, even to the point of modifying the injector face to correspond with the machine shop errors made on the original injector face. Many of the starting methods used have resulted in a unidirectional detonation wave that quenches after the first revolution. Initially, it was believed that this phenomenon was solely due to the fact that the blockage in the combustion chamber was sufficient to stop the propagation of a detonation wave in either direction. However, subsequent experiments indicate that there is heat addition occurring in the combustion chamber between the first revolution of the detonation wave and the closure of the propellant valves. It is impossible, at this time, to determine which of these two processes is the major problem.

In order to solve the starting problem for the 100-lb thrust motor, it is imperative that the development and propagation of a detonation wave be studied. This study must be made at the same conditions that are present in the 100-lb thrust motor, and the study can probably best be performed by optical methods. Therefore, the test section shown in Figure 3(b) has been fabricated and is now ready for testing. The construction of this linear motor is similar to the 100-lb thrust motor, and could be duplicated, except for the plexiglas windows, by cutting the 100-lb thrust motor along a radial line and forming it into a straight test section.

Installation of the linear motor has been quite efficient because it was designed to utilize the same test facility as the 100-lb thrust motor. The initial linear motor test runs will be in the same manner as the gaseous 100-lb thrust motor runs except the run time will be shortened in order to protect the windows.

The major purpose of these tests is to observe the development of the detonation wave and its interaction with the starting mechanism. None of the experiments will be concerned with the gas dynamics of the combustion chamber after the detonation wave reflects from the test section ends, however, some emphasis will be placed on the injector face flow pattern prior to ignition.

The first starting arrangement to be tested will be a spark plug igniter and either a film or brass shim stock blockage in the combustion chamber. The blockage will be placed at various stations in the combustion chamber with emphasis placed on the region where the detonation wave is still in the development stage. The pertinent data to be observed during these tests will be; interaction of the combustion zone with the blockage, duration of the blockage, and the effectiveness of the blockage. If this scheme is successful in establishing a unidirectional detonation wave, the blockage must also be subjected to a fully developed detonation wave in order to determine if the starting mechanism is completely satisfactory.

B. DETONATION THROUGH HETEROGENEOUS LIQUID-GAS MEDIA

In Reference 2 a series of spark-schlieren photographs is presented showing the breakup process of a row of water droplets exposed to the passage of a fully developed, C-J detonation wave under the following conditions:

Droplet diameter	1000 μ
Droplet spacing	3/32 - 1/8 inch
H_2 - O_2 mixture	$X_{H_2} \approx .70$
Magnification	2.5:1

Additional experimental information has been obtained utilizing the same equipment and techniques concerning the breakup process involved with smaller water droplets exposed to detonation waves under the following similar conditions:

Mean droplet diameter	400 - 500 μ
Range in droplet diameter	220 - 580 μ
Droplet spacing	3/32 - 1/8 inch
H_2 - O_2 mixture	$X_{H_2} \approx 2/3$ (stoichiometric)
Initial Pressure	One atmosphere
Initial Temperature	Room temperature
Magnification	2.75:1

The smaller droplets were produced by utilizing a smaller hypodermic tubing than utilized in producing the 1000 μ droplets. Improvements in the optical system which included a focusing vernier adjustment were made in an attempt to obtain more detail with a greater magnification.. An increase in magnification of only 10% was achieved, however, due primarily to two effects. It was necessary to conduct the experiments during daylight hours for this study, consequently, excessive exposure to extraneous light was encountered with the extremely fast film (ASA-3000) employed. In addition, a residue accumulation on the surface of the test section windows occurred which made it increasingly difficult to obtain sufficient light transmission and optical detail. It was essentially for these reasons that the optical quality of the photographs was actually inferior to the earlier photographs presented in Reference 2

The series of photographs taken of the row of droplets at different time intervals after the passage of the wave yields the following information:

The droplets shatter significantly in the time interval of from 5 to 10 μ-sec after the passage of the wave similar to that which was observed for the 1000 μ droplets. This conclusion is arrived at due to the observed increase in the apparent droplet diameter by a factor of three or more in this time interval. It is believed that this apparent increase is due to the shear-type breakup process observed by other investigators in which the opaque zone is actually a region occupied mainly by a very dense population of micro-droplets surrounding the remains of the parent droplet. It is not possible to establish conclusively whether

a portion of the parent droplet still remains after the observed time interval of about 10 μ-sec. What is indicated however, is that the location of the upstream edge of the opaque region is unchanged from the original position of the row of droplets up to about 10 μ-sec after the passage of the wave. In the time interval of from 10 to 15 μ-sec after the passage of the wave, however, a measurable change in the upstream position has occurred for the smaller droplets (originally ~ 300 μ diameter). It indicates that the upstream position of the opaque zone has accelerated to an average velocity in this time interval of the order of 30 to 60 ft/sec. While this is quite low compared to the theoretical gas velocity of about 4200 ft/sec behind a stoichiometric H_2 - O_2 detonation wave, it represents the same order of acceleration as that observed in the shorter time interval (0 to 10 μ-sec) for the downstream edge of the opaque zone—a zone which is believed to be made up of a dense population of micro-droplets.

Figure 4 shows a typical spark schlieren photograph of the row of droplets about 11 μ-sec after the passage of the wave. The detonation wave is just out of the field of view moving to the right. For comparison, a photograph of a typical row of undistrubed droplets is also shown. The closely spaced parallel lines on the left side of the photographs are reference wires spaced . 078 inches apart. The weak normal shock wave just visible upstream of the row of shattered droplets was not evident on the earlier photographs utilizing 1000 μ droplets. Several possible reasons for the appearance of this wave are under consideration.

More refined measurements would be required to establish conclusively whether or not the parent droplets of the order of 200 to 300 μ initial diameter are completely shattered into a spray of micro-droplets in the observed time interval. It is believed, however, that more precise measurements of this type would yield significant information concerning the detailed droplet shattering processes occurring in an actual heterogeneous detonation wave, i. e., a detonation in which the fuel or the oxidizer component of the reactants are originally in the liquid droplet form.

C. GEOMETRICAL TESTS

1. Introduction

These experiments are essentially a conclusion of the work reported in references (1) and (2) concerning the effect of curvature and pressure relief on a fully developed detonation wave. The experiments utilize three geometrical configurations:

(1) A curved channel with the cross-sectional dimensions of 1/2 x 3/8 inch with a radius of curvature of 3.75 inches having complete confinement i.e., solid walls.

(2) A curved channel with the same dimensions as in (1) above except with the elimination of the inner wall allowing a two-dimensional expansion (pressure relief) of the burned gases behind the wave in the inward, radial direction. Provision is made for the placement of a thin amyl acetate film along this inner wall separating the unburned gases from the atmosphere.

(3) The same channel dimensions as in (1) and (2) above with one window removed so that the relief is in the axial direction.

The majority of the experiments utilized a stoichiometric mixture of hydrogen and oxygen.

2. Experimental Test Equipment

A schematic diagram of the basic test section with solid walls is shown in Figure 5 . A photograph of the test section is shown in Figure 6 . The curved section includes 270°. Provision is made for the removal of the inner wall for the full 270°.

A different section including only 90° was utilized for some of the studies of detonations with inward, radial relief. This section has provision for a thin membrane (15% collodion in amyl acetate). Details of the construction and film preparation is given in Reference 2 .

Each curved test section, when used, is attached to a straight detonation tube driver section of the same cross-sectional dimensions as the curved sections. The straight driver section is nine feet long to insure a fully developed detonation wave before entry into the curved section. A miniature glow plug is used for ignition purposes. A schematic diagram of the basic system appears in Figure 7 .

3. Experimental Procedure

The experiments performed in the test section with the solid walls is obtained in the following manner. A diaphragm is used to seal the end of the test section, and the tube and test section are evacuated by means of a vacuum pump. Then the H_2 - O_2 mixture is introduced into the tube and test section from a vessel containing the pre-mixed combustible gases. This vessel is not shown in Figure 7 . The mixture is then ignited.

The experiments performed in the sections employing pressure relief are made in either of two ways:

(1) The H_2 - O_2 mixture from the vessel containing the pre-mixed gases is allowed to flow slowly through the straight tube and test section for at least one minute to purge the air and other gases completely. The valve to the pre-mixed gas vessel is closed and the end of the test section is sealed immediately with masking tape. The mixture is then ignited.

(2) A flowing system of H_2 - O_2 is introduced continually through a mixing tee (Figure 7) and metered by means of sonic orifices in each line. The mixture is ignited with the system flowing. This method was also employed when utilizing the test section with solid walls for reasons discussed later.

For each method, the detonation velocity is measured in the straight tube by means of ionization probes. In addition, the time interval to the spark light discharge is also measured. Two CMC, Model 757 BN time interval counters are employed for the two measurements. To photograph the waves, a schlieren system is used employing six inch diameter mirrors instead of the lens system shown (for simplicity) in Figure 7 . The effective exposure time for the high-voltage, capacitor discharge light source is approximately 0.1 μ-sec.

4. Results

Because of the presence of small leaks, the final experiments utilizing the test section with solid walls employed the flowing system for consistency of results.

In addition, for the experiments exploying pressure relief, the method of charging the tube by first purging and then sealing the end was found undesirable because it was determined that the unburned mixture partially diffuses through the thin membrane in the time interval of about three seconds between the closing of the valve and ignition. This effect was

determined by noting that the degree of wave curvature could be changed by varying the aforementioned time interval. See Figure 24(a) of Reference 2 which shows a wave with relief showing this wave curvature effect.

For this reason the following experiments were performed employing the flowing system. Figure 8 (a) shows a typical schlieren photograph of a detonation wave with inward radial relief provided by utilizing a thin amyl acetate membrane on the inner wall. The wave curvature is quite similar to a wave shown in Figure 8(b) propagating in the curved channel with solid walls. Note that the direction of travel is different for the two waves i. e., the wave in Figure 8 (b) is moving counter-clockwise. On the premise that the degree of wave curvature near the relief boundary is a measure of the degree of confinement of the wave, it is concluded that the confinement provided by the amyl acetate membrane is essentially the same as that provided by the solid walls. It is for this reason that the experiments performed utilizing the membrane were not carried out to conclusion.

A composite distance versus relative time plot of stoichiometric H_2- O_2 detonation waves in the solid walled curved section employing a flowing system is shown in Figure 9 . The distance as shown is obtained by measuring the wave position along the outer wall. It is apparent due to the linear nature of the average of the experimental data that the wave velocity is constant throughout the curved section. The wave velocity obtained from the slope of the average line is 9762 ft/sec. From similar plots the velocity on the inner wall and on the center line are 8541 ft/sec and 9152 ft/sec respectively. The average wave velocity measured in the straight tube before the curved test section is 9159 ft/sec, a value very close to that observed along the center line of the curved section.

A schematic drawing showing the essential features of a typical detonation wave in a curved channel is shown in Figure 10, obtained from typical schlieren photographs similar to Figure 8 (b). Two interesting effects are shown in addition to the curvature of the wave from the radial direction. First, it is noted that stria exist in the burned gases behind the wave characteristic of typical detonations. Also observable are multiply-reflecting shock waves emanating initially from the outer wall intersection with the detonation wave front. It is apparent that such a reflected wave must accompany an oblique shock wave in steady flow. Upon close scrutinization of many original photographs it appears that the observed stria indicate the approximate direction of the streamlines in the burned gases because they are deflected in the same manner as that predicted by two dimensional oblique shock theory. It is concluded therefore that the observed shock system which does not dissipate with the distance travelled by the wave in the curved tube is a characteristic of a steady state detonation in a curved channel.

It is of interest to calculate the theoretical pressure gradient in the radial direction. This quantity is represented by the following relation:

$$\frac{\partial P_2}{\partial r} = \frac{\rho_2 V_2^2}{r} \tag{1}$$

where P_2, ρ_2 and V_2 are the pressure, density and absolute gas velocity in burned gases immediately behind a detonation wave. Using theoretical values for the properties behind a stoichiometric, C-J detonation (initially at 1 atmosphere and room temperature), a value of 63.5 psi/inch is obtained using relation (1). Utilizing the experimental distance of 1/2 inch between the outer and inner wall, a value of about 32 psi is obtained for the overall radial pressure differential theoretically predicted using the 1/2 inch section. It is to be noted that this differential is about 12% of the theoretically predicted pressure, P_2, of 276 psia immediately behind a one-dimensional detonation.

Another method can also be used to predict the radial pressure gradient behind a detonation in a curved channel by utilizing the momentum equation across the wave,

$$\frac{P_2}{P_1} = \frac{1 + \gamma_1 M_1^2}{1 + \gamma_2 M_2^2} \tag{2}$$

where M_1 and M_2 are the Mach number in the unburned and burned cases respectively for a one-dimensional wave. The Mach number normal to the wave which is required by this relation can be obtained from measurements of the wave angle at points along the wave. It was determined from the experiments that the angular deviation of the wave from the radial direction varied from zero at the inner wall to 16.4° at the outer wall. Using relation (2) above, the pressure differential across the channel is calculated to be about 47 psi which compares favorably with the value of 32 psi predicted by Equation (1).

Other tests were made utilizing the 270° curved test section with the inner wall removed and using a flowing stoichiometric mixture of H_2-O_2. Figure 11 is a schlieren photograph of a typical detonation wave in this system. The wave is approximately 250° from the beginning of the curved section. Because of the lack of detail on the photograph, Figure 12 is included as a sketch of the essential details. With the flowing system utilized, a high concentration of combustible mixture is maintained apparently due to centrifugal effects allowing the detonation wave to be sustained. Although some mixing must be occurring between the unburned mixture and the atmosphere, the effect must be small, at least near the beginning of the curved section. Also just visible in Figure 11 is the first reflected wave originating from the intersection of the detonation wave and the outer wall. Multiple reflected shock waves are not observed due to the absence of a reflection from the gaseous interface between the burned gases and the atmosphere.

Figure 13 shows a distance versus relative time plot from a limited number of waves. Again, in a manner similar to the case with the tube having solid walls, the velocity (slope) of the average curve seems to be linear. However, in comparing the detonation velocity at the channel centerline with the velocity obtained previously with a solid wall inner boundary, the velocity obtained with the inner wall removed appears to be about 7.5% lower over the complete length of the curved section. This is rather surprising inasmuch as it would appear that the mixing effect between the unburned gases and the atmosphere would become progressively more noticeable as the wave moves into the curved section. From the experiments, apparently this effect is not measurable over the distance involved, and the degradation of about 7.5% in the detonation wave velocity is actually due primarily to the relief effect of the unconfined gases behind the detonation wave. It is to be noted that certain theoretical and experimental results of a similar study* underway at this laboratory utilizing detonations with relief in straight tubes tend to support these observations.

Figure 14 shows a schlieren photograph of a detonation wave propagating in a channel with one window removed so that in effect an expansion of the burned gases takes place in the axial direction. The wave has passed through the first four inches of the curved section. It is apparent from the photograph that the detonation wave has degenerated into a curved shock front followed by the combustion zone (indicated by the turbulent region beginning about 1/4 inch behind the initial shock wave). It is quite possible that the detonation wave is in the process of being quenched due to the mixing processes which could be more pronounced for this case where centrifugal effects are not encountered in the same stabilizing manner as in the case with the inner wall removed.

5. Conclusions

(1) In general it can be stated that in curved channels of rectangular crossection (of the same approximate dimensions as that utilized here) detonation waves will propagate at velocities (measured at the channel centerline) equal to that observed in straight tubes.

(2) With pressure relief on the inner wall, measured detonation velocities in the curved channel appear to suffer a degradation of no more than 7.5% compared to the measured velocities of completely confined waves. With a very thin, amyl acetate membrane separating the unburned gases from the atmosphere along the inner wall of a curved channel, possibly no degradation in velocity will be encountered.

---

*Dabora, E., unpublished work in progress at this laboratory.

(3) Further detailed studies would certainly be warranted with more carefully controlled procedures and conditions than utilized in these experiments.

III. STUDY PLANS FOR THE NEXT QUARTER

The theoretical studies involving the simplified model will be essentially completed with the results of the numerical computations of the modified model now in progress. The results of the study will be applied to sizing considerations for the nominal 1000-lb thrust motor. The validity of the theoretical model will be examined when experimental results from the 100-lb thrust motor are available.

The work involving the 100-lb thrust motor will be suspended until a reasonable solution to the starting problem is obtained. The linear motor with transparent walls will be utilized for this purpose. Following this, a performance study utilizing the basic 100-lb thrust motor will be initiated. Emphasis will be placed on the possibility of upgrading the entire experimental system involved to obtain a nominal 1000-lb thrust from the gaseous motor.

REFERENCES

1. Nicholls, J. A., and Cullen, R. E., et al., The Feasibility of a Rotating Detonation Wave Rocket Motor, Univ. of Mich. Eng. Res. Inst., Report 05179-2-P, Dec. 1962.

2. Nicholls, J. A., and Cullen, R. E., et al., The Feasibility of a Rotating Detonation Wave Rocket Motor, Univ. of Mich. Eng. Res. Inst., Report 05179-3-P, Mar. 1963.

3. Courant, R., and Friedricks, K. O., Supersonic Flow and Shock Waves, Interscience Publishers, Inc., New York, 1948, pp. 121-124.

4. Zeleznik, F. J., and Gordon, S., A General IBM 704 or 7090 Computer Program for Computation of Chemical Equilibrium Compositions, Rocket Performance, and Chapman-Jouguet Detonations, NASA TN D-1454, Oct. 1962. (Note: Some results for stoichiometric Chapman-Jouguet detonations are presented in "Calculation of Detonation Properties and Effect of Independent Parameters on Gaseous Detonations," ARS Journal, 32, 606 (1962).)

Solution to the no mixing case:

$G = 1.0$
$\bar{T}_P = 0.081$
$\gamma_A = 1.401$
$\gamma_B = 1.15$
$\bar{C}_{P_A} = 0.5497$

The dependent parameters satisfying both the differential equations and the hydrodynamic jump conditions are:

$B = 5.76$
$\bar{V}_W = 1.797$
$\bar{Q} = 0.788$

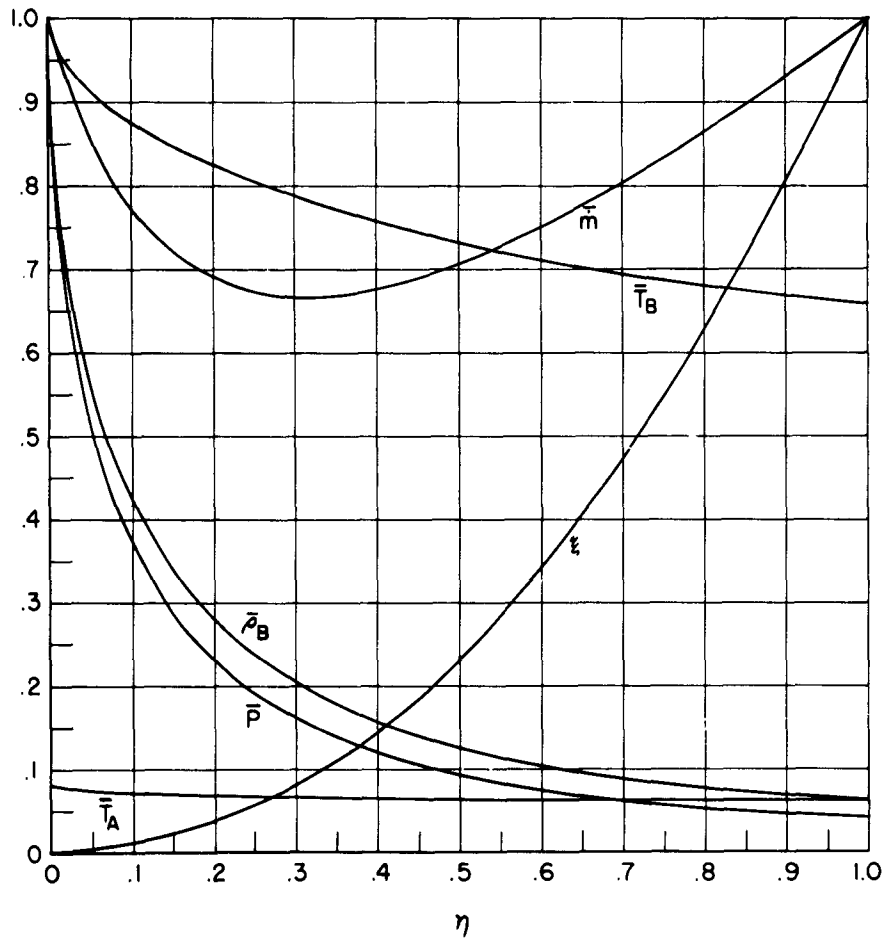

Figure 1 (a). Dimensionless Properties $\bar{P}$, $\bar{T}_A$, $\bar{T}_B$, $\bar{\rho}_B$, ξ, and $\bar{m}$ as Functions of the Dimensionless Circumferential Coordinate, η, for $\bar{T}_P = 537^{\circ}R$, Gaseous No Mixing Case.

Solution to the no mixing case:

$G = 1.0$

$\bar{T}_P = 0.081$

$\gamma_A = 1.401$

$\gamma_B = 1.15$

$\bar{C}_{P_A} = 0.5497$

The dependent parameters satisfying both the differential equations and the hydrodynamic jump conditions are:

$B = 5.76$

$\bar{V}_W = 1.797$

$\bar{Q} = 0.788$

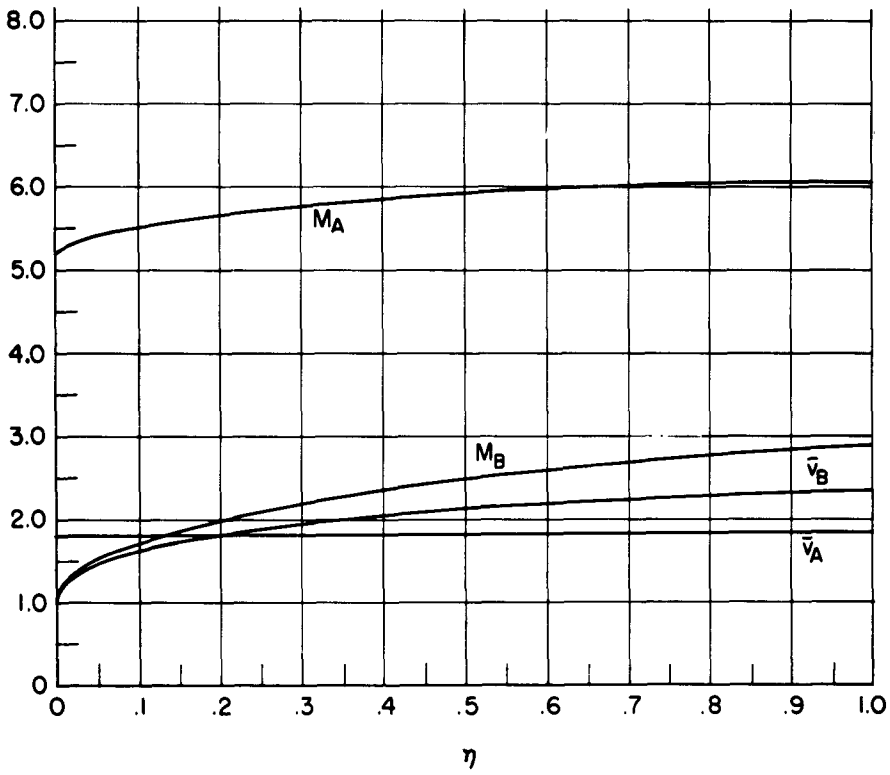

Figure 1 (b). Dimensionless Properties M_A, M_B, $\bar{v}_A$, $\bar{v}_B$ as Functions of the Dimensionless Circumferential Coordinate, η, for $\bar{T}_P = 537^{\circ}R$, Gaseous No Mixing Case.

Solution to the no mixing case:

$G = 1.0$
$\bar{T}_P = 0.04075$
$\gamma_A = 1.5$
$\gamma_B = 1.15$
$\bar{C}_{P_A} = 0.4923$

The dependent parameters satisfying both the differential equations and the hydrodynamic jump conditions are:

$B = 7.608$
$\bar{V}_W = 1.8303$
$\bar{Q} = 0.8037$

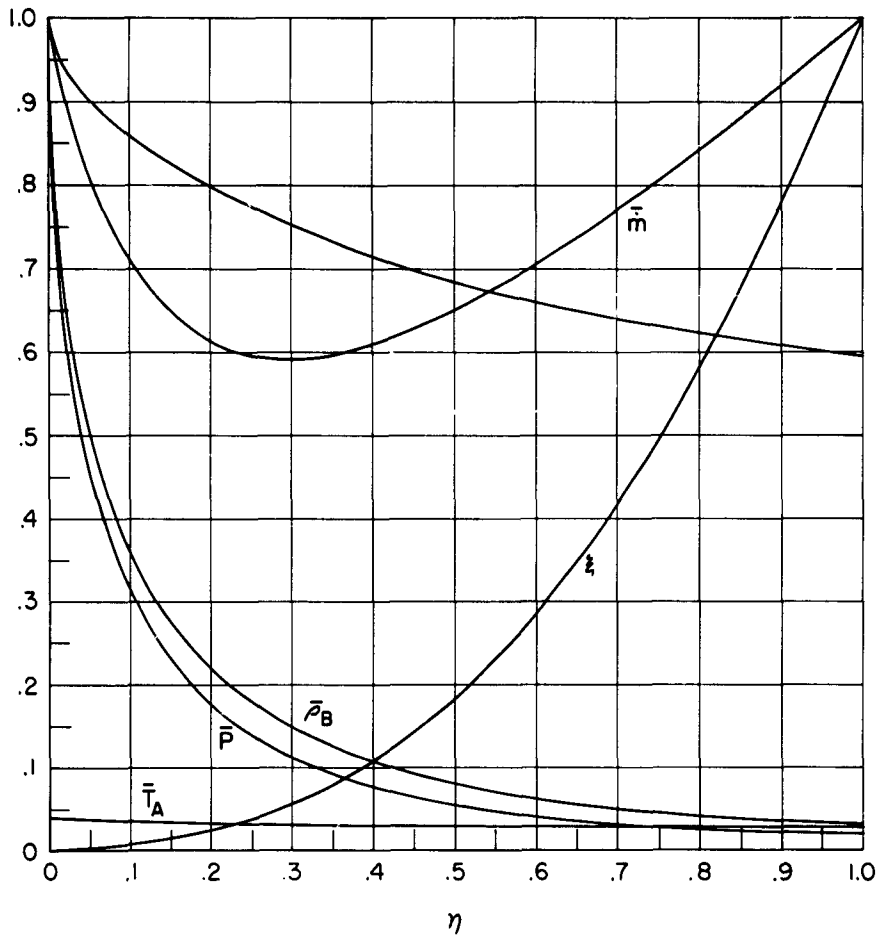

Figure 2 (a). Dimensionless Properties $\bar{P}$, $\bar{T}_A$, $\bar{T}_B$, $\bar{\rho}_B$, ξ, and $\bar{m}$ as Functions of the Dimensionless Circumferential Coordinate, η, for $\bar{T}_P = 270^0$R, Gaseous No Mixing Case.

Solution to the no mixing case:

$G = 1.0$

$\bar{T}_P = 0.04075$

$\gamma_A = 1.5$

$\gamma_B = 1.15$

$C_{P_A} = 0.4923$

The dependent parameters satisfying both the differential equations and the hydrodynamic jump conditions are:

$B = 7.608$

$\bar{V}_W = 1.8303$

$\bar{Q} = 0.8037$

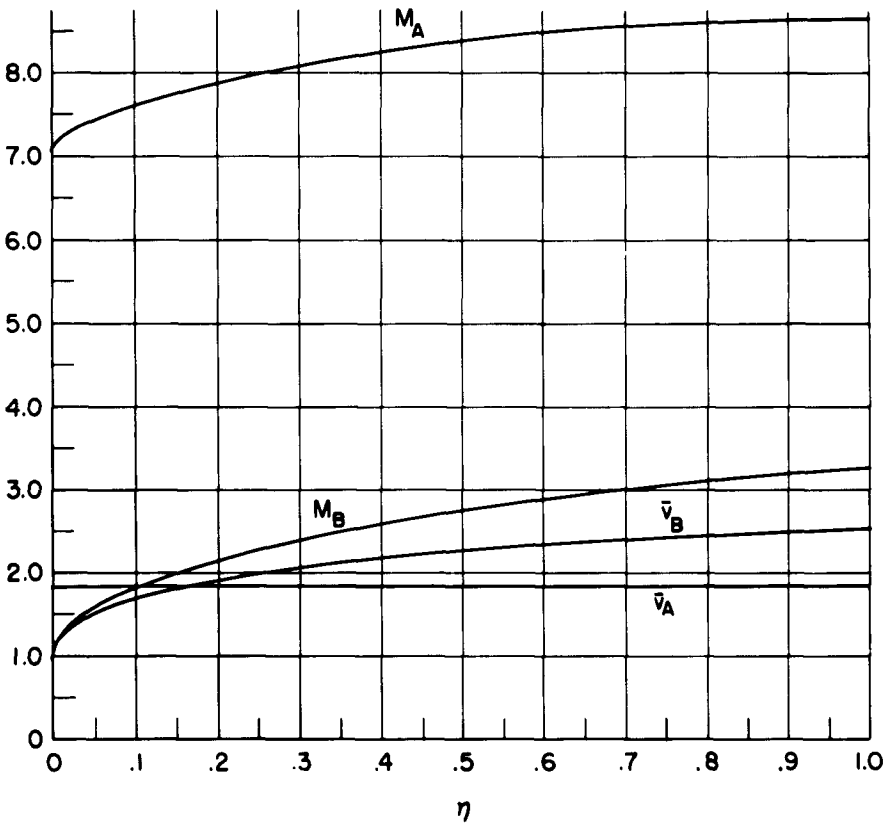

Figure 2 (b). Dimensionless Properties M_A, M_B, $\bar{v}_A$, $\bar{v}_B$ as Functions of the Dimensionless Circumferential Coordinate, η, for $\bar{T}_P = 270^{\circ}R$, Gaseous No Mixing Case.

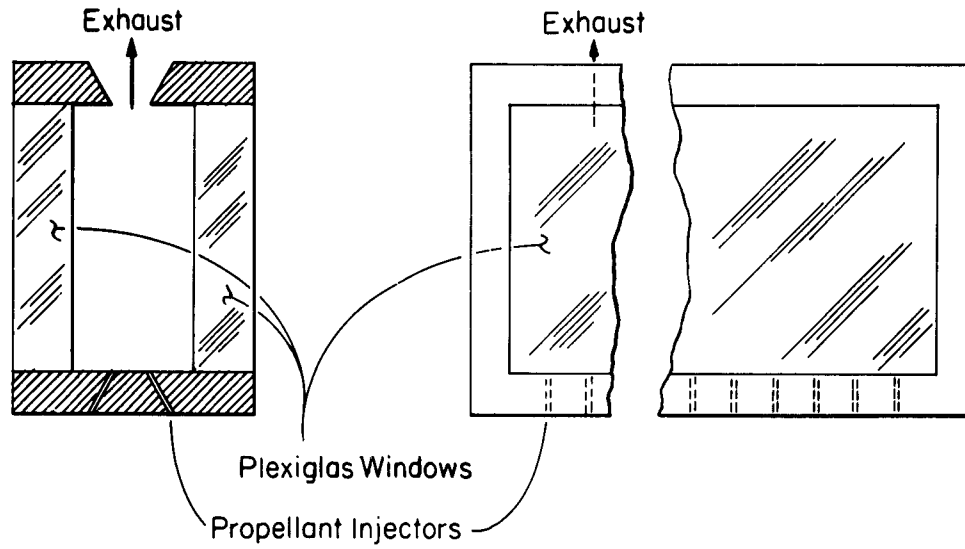

Figure 3 (a). Schematic View of the Linear Motor.

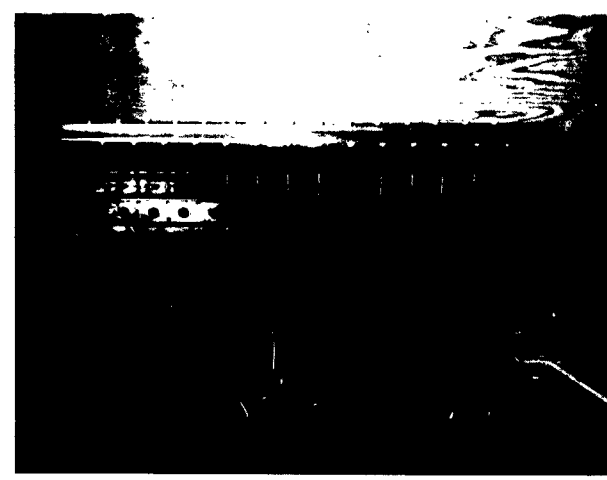

Figure 3 (b). Photograph of the Linear Motor on the Test Stand.

(a)

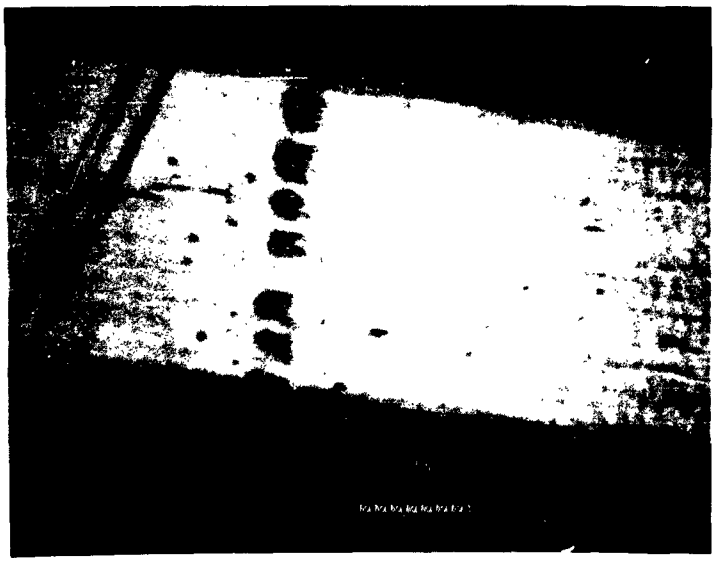

(b)

Figure 4. Schlieren Photographs of the Shattering of H_2O Droplets Behind an H_2 - O_2 Detonation Wave ($X_{H_2} \approx .67$).

(a) Undisturbed Droplet Row (220-580 μ Diameter) (Retouched)

(b) Shattered Droplets 11-12 μ-sec After Passage of Wave.

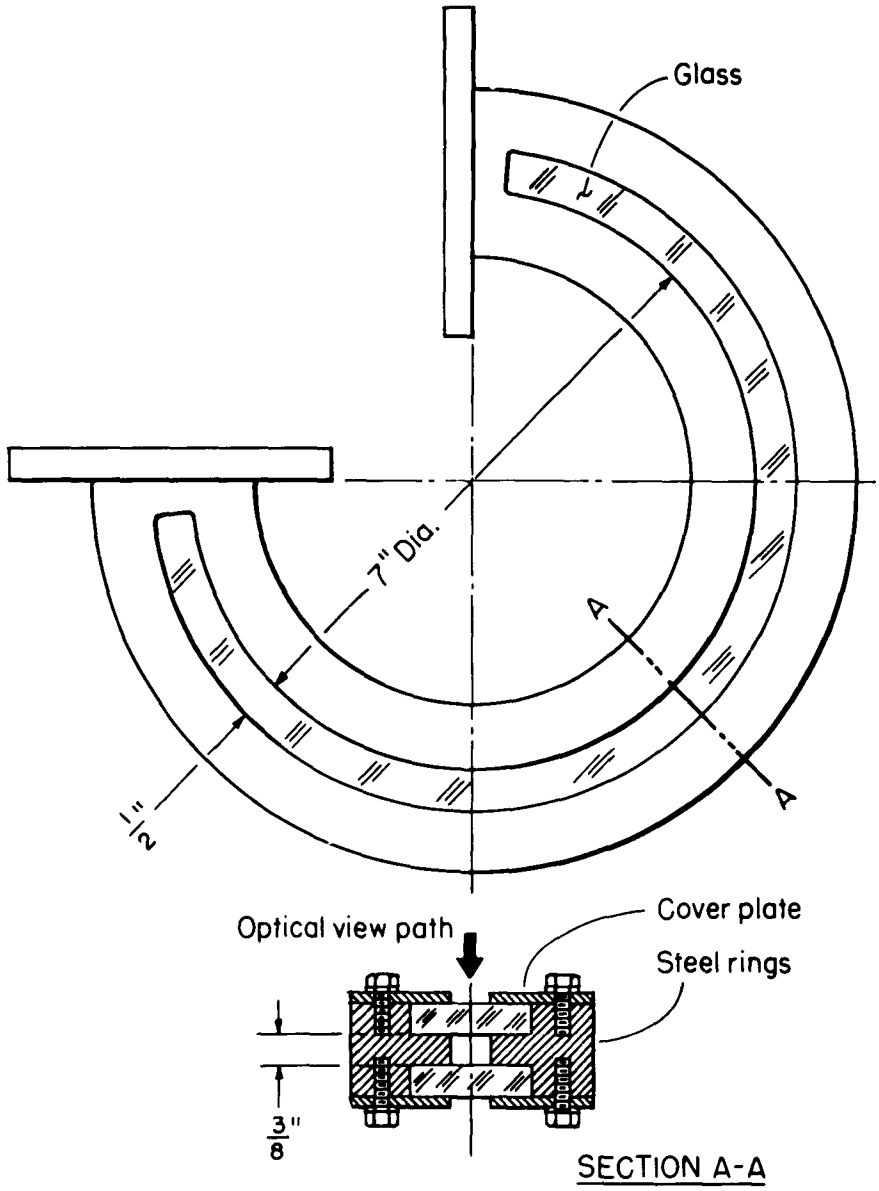

Figure 5. Schematic Drawing of the Curved Detonation Tube Section with Solid Walls.

Figure 6. Photograph of the Curved Detonation Tube Section with Solid Walls.

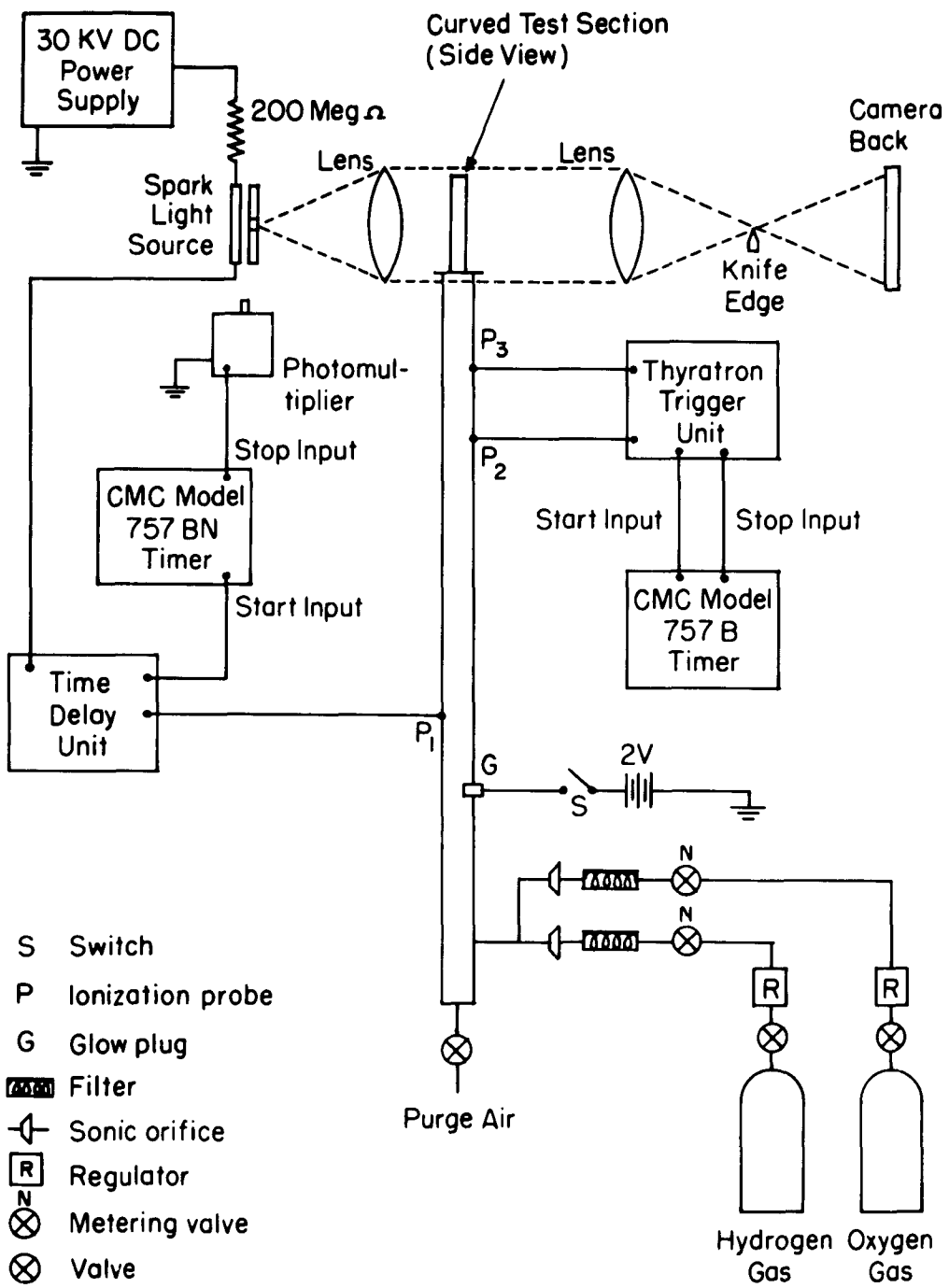

Figure 7. Schematic Diagram of the Basic Experimental System for Studying Detonation Waves in Curved Channels.

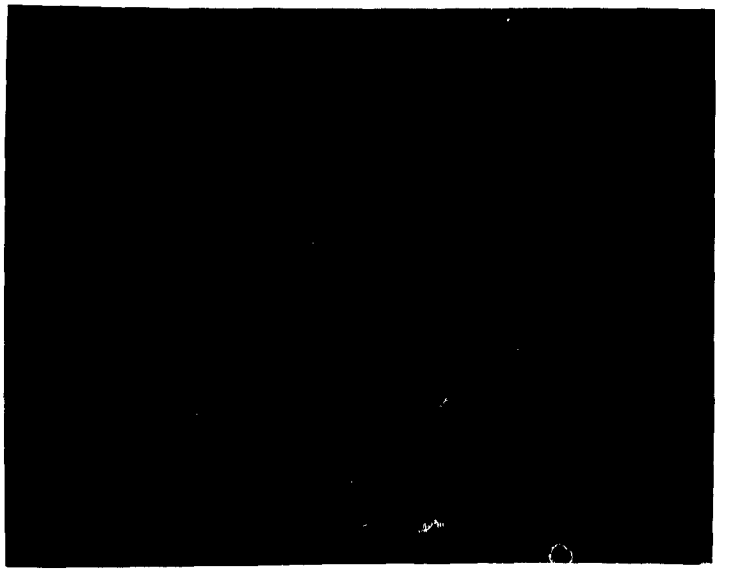

Figure 8 (a). Schlieren Photograph of a Stoichiometric H_2 - O_2 Detonation Wave in a Curved Channel Utilizing a Thin, Amyl-Acetate Membrane for Inward Radial Relief Employing a Flowing System.

Figure 8 (b). Schlieren Photograph of a Stoichiometric H_2 - O_2 Detonation Wave in a Curved Channel with Complete Solid Wall Confinement Employing a Flowing System.

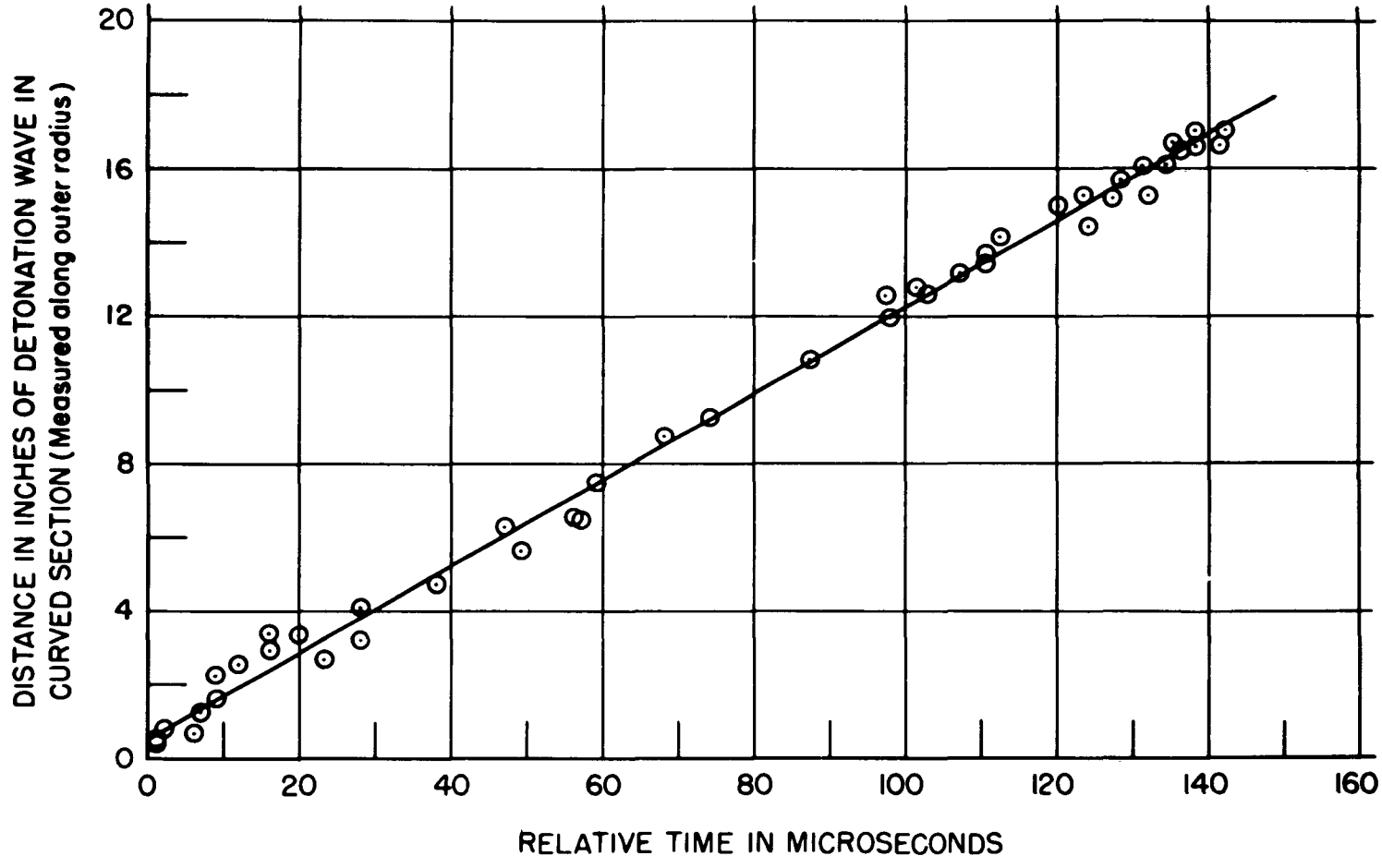

Figure 9. Position Versus Relative Time of Stoichiometric H_2 - O_2 Detonation Waves Along the Outer Radius of the Curved Channel with Complete Solid Wall Confinement Employing a Flowing System.

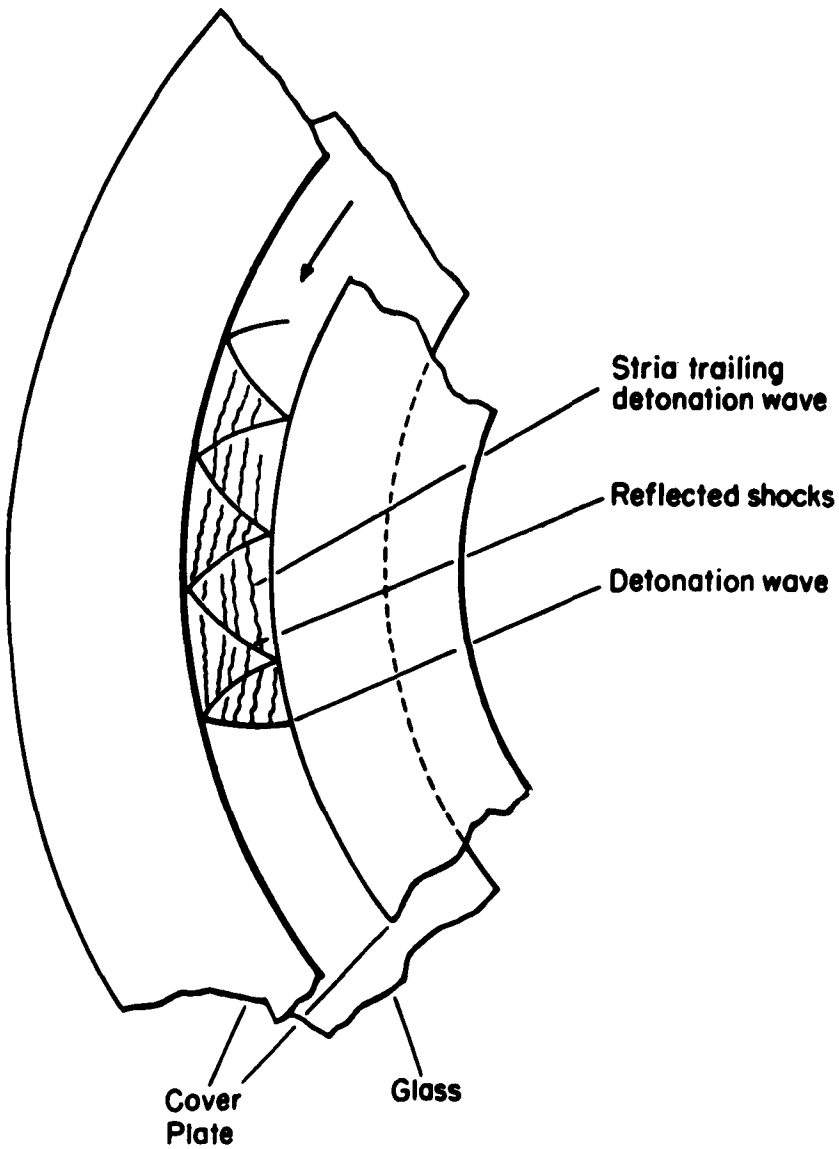

Figure 10. Interpretive Sketch of a Stoichiometric H_2 - O_2 Detonation Wave in a Curved Channel with Complete Sclid Wall Confinement.

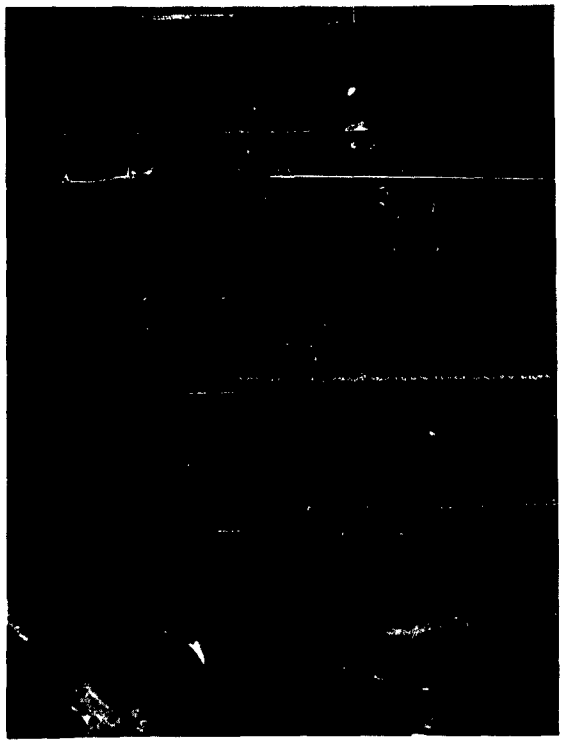

Figure 11. Schlieren Photograph of a Stoichiometric H_2 - O_2 Detonation Wave in a Curved Channel with the Inner Wall Removed Employing a Flowing System.

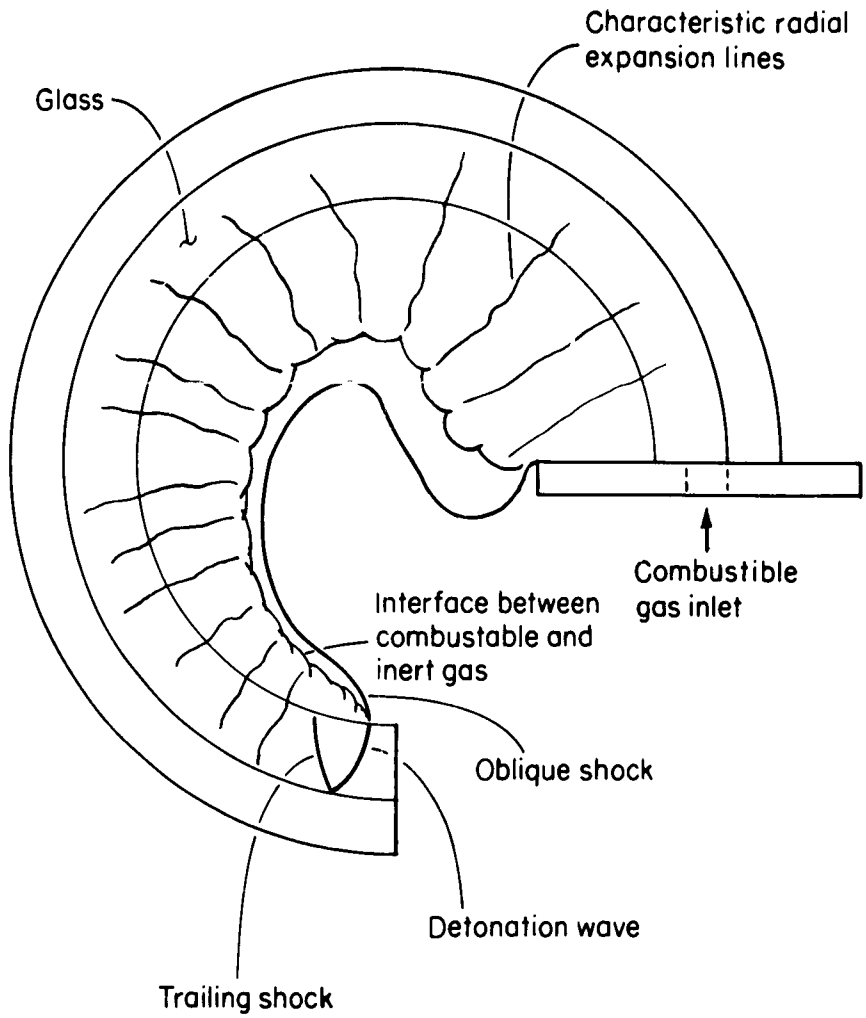

Figure 12. Interpretive Sketch of a Stoichiometric H_2 - O_2 Detonation Wave in a Curved Channel with the Inner Wall Removed Employing a Flowing System.

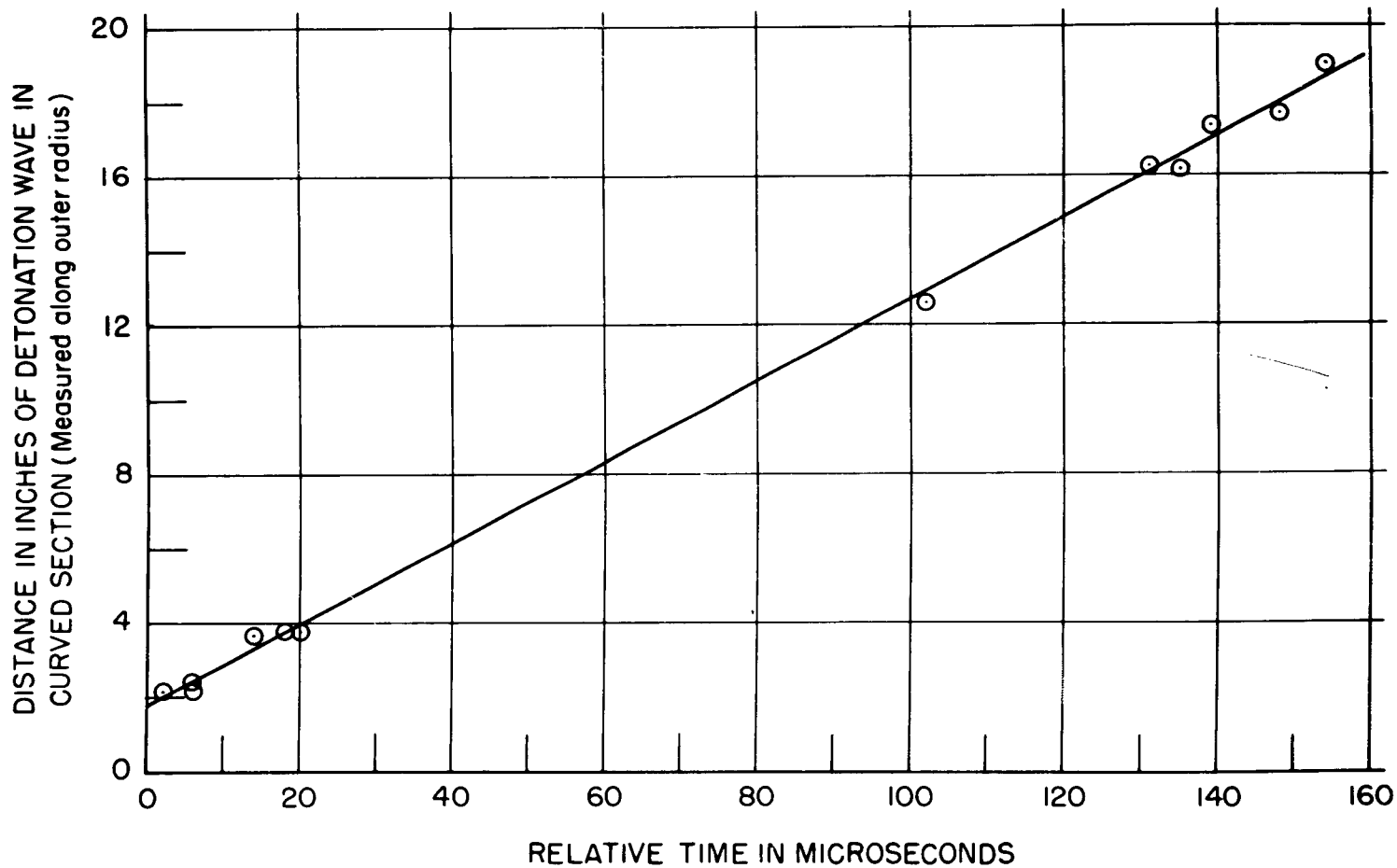

Figure 13. Position Versus Relative Time of Stoichiometric H_2 - O_2 Detonation Waves Along the Outer Radius of the Curved Channel with Inner Wall Removed Employing a Flowing System.

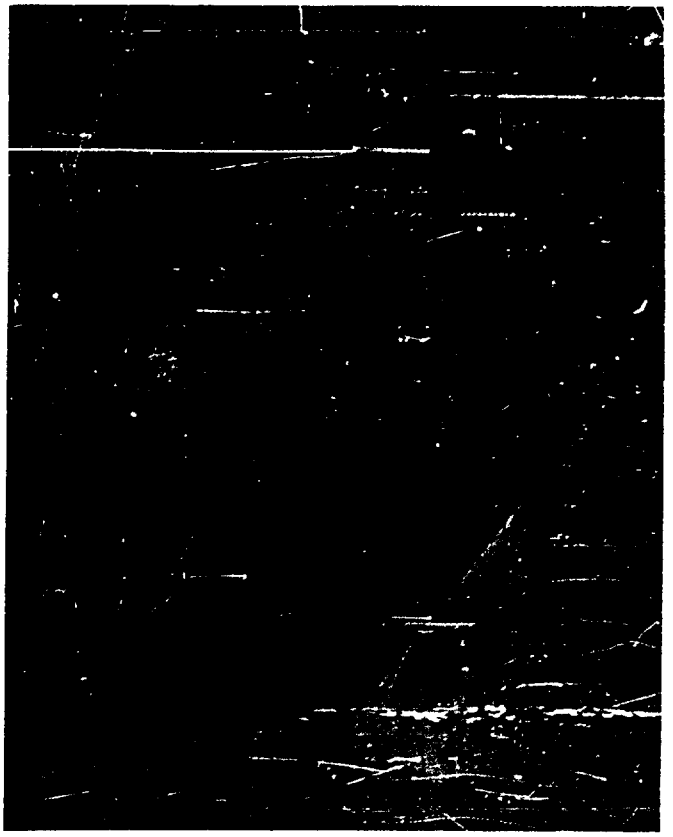

Figure 14. Schlieren Photograph of a Stoichiometric H_2 - O_2 Detonation Wave in a Curved Channel with One Window Removed (Relief in the Axial Direction).